Journal of Thrombosis and Haemostasis, **11** (Suppl. 1): 36–45 DOI: 10.1111/jth.12254

INVITED REVIEW

Innovation in detection of microparticles and exosomes

E. VAN DER POL,*†[1] F. COUMANS,*†[1] Z. VARGA,‡ M. KRUMREY§ and R. NIEUWLAND*

*Laboratory of Experimental Clinical Chemistry; †Biomedical Engineering & Physics Academic Medical Centre of the University of Amsterdam, Amsterdam, the Netherlands; ‡Biological Nanochemistry, Institute of Molecular Pharmacology, Research Centre for Natural Sciences of the Hungarian Academy of Sciences, Budapest, Hungary; and §Physikalisch-Technische Bundesanstalt (PTB), Berlin, Germany

To cite this article: van der Pol E, Coumans F, Varga Z, Krumrey M, Nieuwland R. Innovation in detection of microparticles and exosomes. *J Thromb Haemost* 2013; **11** (Suppl. 1): 36–45.

Summary. Cell-derived or extracellular vesicles, including microparticles and exosomes, are abundantly present in body fluids such as blood. Although such vesicles have gained strong clinical and scientific interest, their detection is difficult because many vesicles are extremely small with a diameter of less than 100 nm, and, moreover, these vesicles have a low refractive index and are heterogeneous in both size and composition. In this review, we focus on the relatively high throughput detection of vesicles in suspension by flow cytometry, resistive pulse sensing, and nanoparticle tracking analysis, and we will discuss their applicability and limitations. Finally, we discuss four methods that are not commercially available: Raman microspectroscopy, micro nuclear magnetic resonance, small-angle X-ray scattering (SAXS), and anomalous SAXS. These methods are currently being explored to study vesicles and are likely to offer novel information for future developments.

Keywords: exosomes, flow cytometry, microparticles, raman spectroscopy, secretory vesicles.

Introduction

Cell-derived (extracellular) vesicles contain a phospholipid bilayer and have diameters ranging from 50 nm to 5 μm [1]. We will use the term 'vesicles' for all vesicles in human body fluids and culture media because no consensus exists on nomenclature and classification [1]. The scientific and clinical interest in vesicles is increasing as they contribute to health and disease processes and are potentially useful as biomarkers and therapeutic agents.

The detection of vesicles is extremely challenging because many vesicles have a diameter of less than 100 nm, have a low refractive index, are highly heterogeneous [2], and are sensitive to collection and handling conditions [2–7]. Detection limitations have practical consequences because methods such as flow cytometry have been pushed to their limits, resulting not only in improved detection but also in measurement of artefacts.

Vesicles have been studied extensively by electron microscopy and functional (coagulation) assays since the 1950′s. Many investigators, including ourselves, have used flow cytometry for the detection of vesicles since the 1990′s, but owing to the use of novel technologies, such as nanoparticle tracking analysis (NTA), dynamic light scattering (DLS), and resistive pulse sensing (RPS), we have learned that many vesicles are too small to be detected as single vesicles by flow cytometry. Since then, the detection of vesicles has gained considerable interest, and at present, a plethora of detection methods are being explored and no gold standard exists for the detection of vesicles. In parallel, attempts are being made to standardize vesicle measurements and pre-analytical variables.

To illustrate the presence and dimensions of vesicles in body fluids, Fig. 1A shows a size distribution of vesicles in 1 mL platelet-free plasma after a single freeze/thaw cycle, measured with NTA (Nanosight, Amesbury, UK). The total number of particles/vesicles in this sample is 7.3×10^{10}/mL, with a total surface area of 22 cm^2 (Fig. 1B) and a total volume of 73 nL (Fig. 1C). Thus, the total volume of the particle/vesicles is approximately 85-fold less than of leukocytes in 1 mL of blood, whereas the total surface area is comparable.

Please also note that the size of vesicles is within a range of easily detectable contaminants such as immune complexes [8–10], calcium-phosphate microprecipitates [11], liposomes and other particles [12], and fluorescent antibody aggregates [13], which may introduce artefacts in any of the techniques described in this review. For example, we can erroneously reproduce the finding that 'platelet-derived microparticles' are present in synovial fluid, but only when we do not remove the fluorescent antibody aggregates before labeling of the vesicles [14,15]. The distributions shown in Fig. 1 may be affected by the presence of contaminants. Nevertheless, Fig. 1 illustrates

Correspondence: Rienk Nieuwland, Department of Clinical Chemistry, Academic Medical Centre of the University of Amsterdam, Meibergdreef 9 (Room B1-234), Amsterdam 1105 AZ, the Netherlands.
Tel.: +31 20 5664851; fax: +31 20 6091222.
E-mail: r.nieuwland@amc.uva.nl

[1]Both authors equally contributed to this manuscript.

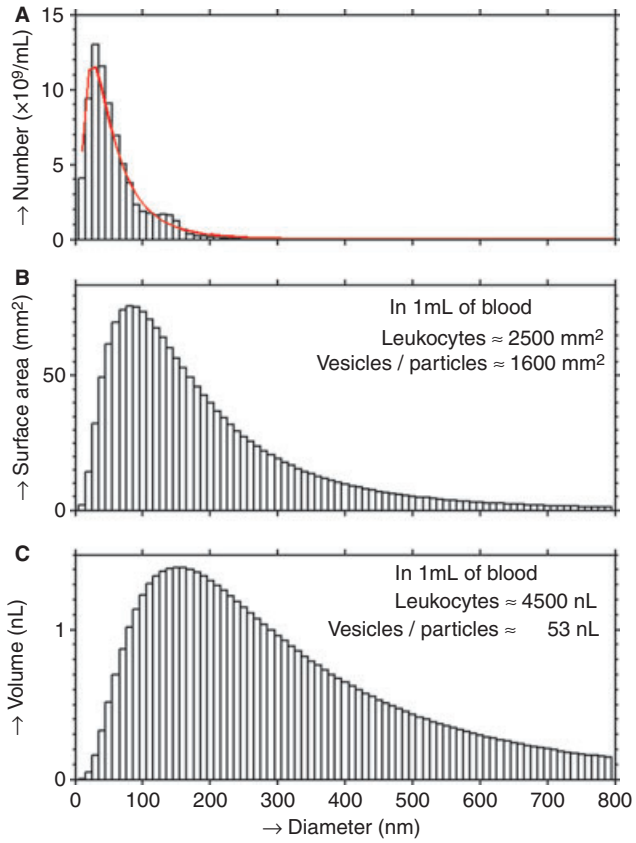

Fig. 1. Properties of vesicles in plasma. (A) Distribution of particle/vesicle sizes present in 1 mL plasma (histogram bin width 10 nm) and a log-normal distribution that was least squares fit to the data (red line). The log-normal fit was used to derive the distribution of vesicle surface area (B) and total vesicle volume (C) per 10 nm bin. For comparison, the total surface area/volume of 5×10^6 leukocytes is shown in panels B and C.

that vesicle measurements require instruments capable of detecting the majority of such particles/vesicles in a large size range.

In this manuscript, we focus on the detection of vesicles free in suspension by commercially available instruments capable of detection at relatively high throughput, that is, time of analysis is minutes per sample under normal conditions. Consequently, new detection methods requiring binding of vesicles to a surface [16,17] are not discussed and have been summarized elsewhere [2]. We will discuss the limitations and shortcomings of each type of instrument, and, in addition, we will present and discuss methods, which are not yet commercially available, but are likely to offer new and relevant information and directions for future research.

Generally available techniques

Flow cytometry

Flow cytometry is well known for multiparameter measurements of single cells at a flow rate of thousands per second. For each cell, the forward and side scatter signals as well as up to nine fluorescence signals can be detected. Flow cytometry is the most commonly applied optical method to detect vesicles in clinical samples because it is the most widely available tool in clinical laboratories to investigate single particles in body fluids [18]. The major challenge for flow cytometry is the detection of single vesicles with a diameter less than the present detection limit [19].

A schematic representation of a flow cytometer is shown in Fig. 2. A hydrodynamically focused sample stream passes through a laser beam. The intersection between the laser beam and the sample stream is the detection volume. When a cell in the sample stream passes through the detection volume, the cell generates scatter and fluorescence signals. A detector in line with the laser beam detects forward scatter signal (FSC), and a wide collection angle objective perpendicular to the laser beam collects side scatter (SSC) and fluorescence. For cells, which are large compared with the laser wavelength, FSC is related to the cell diameter and SSC depends on the presence of subcellular structures. For cells, FSC is much larger than SSC, which means that the FSC detector requires, and typically has, a lower sensitivity than the SSC detector. For vesicles small compared with the laser wavelength, scatter is approximately equal in all directions, and both FSC and SSC are primarily related to vesicle diameter [19,20].

Scatter is determined by the diameter, refractive index, absorption, and morphology of the vesicle, and the laser wavelength [21]. Typically, the vesicle is assumed to be a smooth sphere without absorption, allowing for the application of Mie theory to determine the particle diameter from a known laser wavelength and an assumed refractive index. Fig. 3 shows how the diameter of vesicles, silica beads, and polystyrene beads is related to the SSC signal

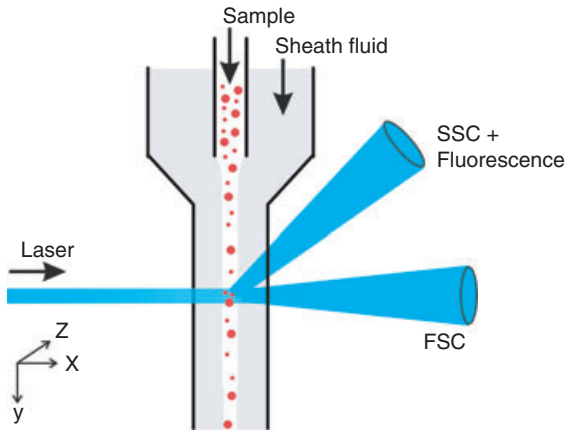

Fig. 2. Schematic representation of a flow cytometer The sample flows from top to bottom and is surrounded by sheath fluid. The laser intersects with the sample stream, generating scatter, and fluorescence signals. Fluorescence and side scatter (SSC) are collected perpendicular to laser beam and sample stream. Forward scatter (FSC) is collected in line with the laser beam.

in a FACSCalibur (BD biosciences, Franklin Lakes, NJ, USA). In principle, this relation can be used to determine the diameter of a particle using the SSC detector. For example, a signal of 10^{-6} W on the SSC detector could be generated by a 130 nm polystyrene bead, a 200 nm silica bead, or a single 240–580 nm vesicle. The latter range is caused by uncertainty in the refractive index of vesicles, with a small range in refractive index from 1.36 to 1.40 (Fig. 3). Recently, the refractive index range of vesicles was estimated to range between 1.36 and 1.45 [22], which would result in a size estimate of 190–1040 nm corresponding to a signal of 10^{-6} mW in Fig. 3. The 5.5-fold uncertainty in size caused by the uncertainty of refractive indices is large compared with the relatively narrow size distribution of vesicles [19].

In a typical flow cytometer, single polystyrene beads with a diameter of 300–500 nm can be detected [23–25]. Novel commercial flow cytometers have a higher SSC sensitivity, and the smallest detectable single polystyrene bead is currently 100 nm [26–28], which corresponds to a single vesicle with a diameter of 160–220 nm (Fig. 3, range of refractive index cytosol 1.36–1.40). The relationship between SSC and diameter depends on the optical configuration of the instrument, including laser alignment, which may change over time. In practice, however, the relationship is not straightforward to obtain and no standardized method for converting SSC to size exists. Therefore, this procedure is still being discussed [18,26,29,30]. An additional complication with the procedure of size calibration using 500 and 900 nm polystyrene beads is that they correspond to different vesicle sizes on different flow cytometers. If we assume a refractive index of cytosol of 1.38 [31], the 500–900 nm range from polystyrene beads corresponds to a vesicle range of 1000–1750 nm when detected using FSC on a Beckman Coulter FC500, 1250–2000 nm when detected using FSC on an Apogee A40 [19], while it corresponds to a range of 2300–4600 nm when detected using SSC on a Becton Dickinson FACSCalibur.

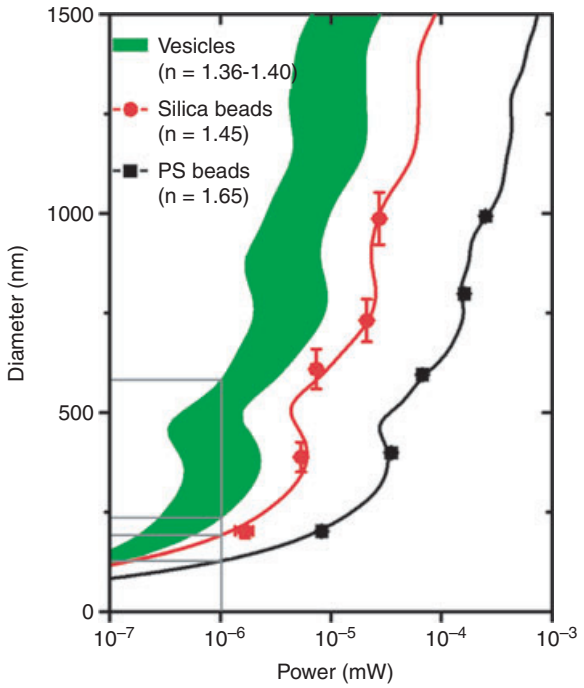

Fig. 3. Relationship between diameter and side scatter The diameter of a vesicle can be derived from side scatter (SSC) when the refractive index (n) is known. SSC for polystyrene beads (PS, black markers) and silica beads (red markers) of known diameter and refractive index was used to fit the SSC vs. diameter relationship (Mie theory, solid lines). This was extrapolated for vesicles with a lipid membrane with refractive index of 1.48 and a cytosol with refractive index of 1.36–1.40 (green band). A signal of 10^{-6} mW is generated by 130 nm PS, 200 nm silica, or 240–580 nm vesicles.

Size determination independent of the refractive index of vesicles can be achieved by applying resistive pulse sensing (RPS), which can be combined with flow cytometry [32]. Nomenclature used for RPS in flow cytometry includes 'impedance based flow cytometry' or the 'Coulter principle'. When a fluid containing vesicles flows through an aperture, the electrical resistance of the aperture increases when a vesicle is present. Although an appropriate choice of aperture allows sizing of cells, vesicles, and even molecules [33], a smaller aperture needed for smaller vesicles also increases the risk of clogging. At this time, no commercial flow cytometry systems are available with RPS sensing apertures suitable for vesicle detection. The Multisizer 3 (Beckman Coulter, Brea, CA, USA) can detect vesicles that occupy 3% of the aperture diameter [34]. With two symmetric RPS channels on a microfluidic chip and a differential amplifier, this detection limit can be reduced to 1% [34,35]. To reduce clogging, the effective sampling aperture can be reduced without reducing the actual aperture by reducing the conductivity of the sheath flow [36,37]. With the differential amplifier, or the less conductive sheath fluid, a pore in the order of 5 μm enables the sizing of single vesicles with a diameter of 50 nm to 5 μm.

Applicability and limitations The size distribution of vesicles (Fig. 1) shows that many vesicles in plasma have a diameter < 100 nm. A flow cytometer that has a detection limit of 200 nm polystyrene beads can detect individual vesicles > 720 nm, which represents < 6% of the total vesicle volume/surface area (Figs 1 and 3).

With the vast majority of vesicles being smaller than the detection limit of current state of the art flow cytometers, the question arises whether these 'undetectable' vesicles contribute to the measurement. Two recent papers demonstrate that the simultaneous presence of multiple undetectable vesicles within the detection volume can produce a signal exceeding the detection threshold and is interpreted as a single vesicle [19,38]. The detection volume of a FACSCalibur flow cytometer is approximately 50 pL [6], which is a suitable size for detection of cells. At a typical vesicle concentration of 10^{10}/mL plasma

[12,16], approximately 500 vesicles are simultaneously present within the detection volume. If the combined SSC from these vesicles exceeds the trigger threshold, for example, because one of the vesicles is relatively large, parameters are recorded for this group of vesicles as if they are a single vesicle. This effect has been termed 'swarm detection' [19]. Swarm detection is easily recognized by measuring a sample at different dilutions [38] and allows detection of vesicles below the detection limit. Importantly, the double-staining with fluorescently labeled markers of vesicles for two or more antigens can be due to the simultaneous presence of two vesicles within the detection volume, each vesicle exposing one of the antigens [19]. With bright fluorescent staining, triggering on fluorescence may be less susceptible to artefacts, because a single vesicle that is too small to be detected by SSC may still be detectable by its fluorescence [38].

New developments Recently, the feasibility of fluorescent detection of vesicles stained with the membrane intercalating dye PKH67 was demonstrated [39,40]. The flow cytometer optical configuration was improved by installing a 200 mW 488 nm laser, a wide-angle FSC detector and a high-performance photomultiplier tube. These changes allow detection of 100 nm polystyrene beads in FSC, which has an improved size discrimination compared with SSC [39]. The staining with PKH67 was followed by removal of unbound dye as well as dye aggregates in a sucrose density gradient. The PKH67 staining can be combined with fluorescent antibody labeling. As the total procedure takes up to 24 h [39], it is an exemplary flow cytometry protocol but in its present form too laborious for routine use. Implementation of RPS, wide-angle FSC, high-performance photon multiplier tubes, and increased irradiance will lead to further improvements of flow cytometry for vesicle analysis.

Dynamic light scattering

Dynamic light scattering (DLS), also known as photon correlation spectroscopy or quasi elastic light scattering, determines the differential size distribution of particles ranging in diameter between 1 nm and 6 μm [41,42]. The sample is illuminated with a laser beam, and therefore, all vesicles present in the beam will scatter light. The size distribution of these vesicles is obtained by measuring the intensity fluctuations of the scattered light, followed by applying a mathematical model derived from Brownian motion and light scattering theory. The absolute concentration of vesicles cannot be determined with DLS because the mean signal amplitude depends on the diameter, concentration, and refractive index of the vesicles.

Many commercial DLS instruments can also determine the zeta potential, which is the electric potential difference between the stationary layer of ions that is bound to the vesicle and the medium.

Applicability and limitations In general, commercial DLS instruments are practical in use. A measurement is typically performed within 1 min and requires sample volumes as low as 20 μL. Accurate size distributions are expected for *mono*disperse samples, that is, samples containing vesicles of one particular size [43–45]. However, size distributions of *poly*disperse samples, such as vesicles in human plasma, are less exact and require foreknowledge of the sample to apply the most suitable mathematical model [43,44]. For example, it is expected that size distributions of polydisperse samples are biased toward small numbers of large particles [44,45], such as platelets and other contaminants, because such particles scatter light more efficiently than small vesicles. Therefore, DLS typically obtains a more than twofold increase in the median diameter of vesicles from plasma compared with other novel techniques [6,12,16,46,47]. We conclude that DLS requires careful data interpretation and may be a useful method provided that the shape of the size distribution is known.

Resistive pulse sensing

Resistive pulse sensing (RPS) determines the absolute size distribution of vesicles in suspension ranging in diameter between ~50 nm and 10 μm by utilizing the Coulter principle [48]. Resistive pulse sensors capable of measuring smaller particles do exist [49], but such instruments are very specialized. This text mainly focuses on a commercial instrument named qNano (Izon Science Ltd, Christchurch, New Zealand). Fig. 4A shows a schematic representation of RPS, which consists of two fluid cells divided by a non-conductive membrane. An electrical current flows through a single pore in the membrane with a diameter typically < 1 μm. Fig. 4B shows the current vs. time when two vesicles from plasma successively pass through the pore. The relative change in current is approximately proportional to the volume of the vesicle and is calibrated with beads of known diameter, a procedure that has been

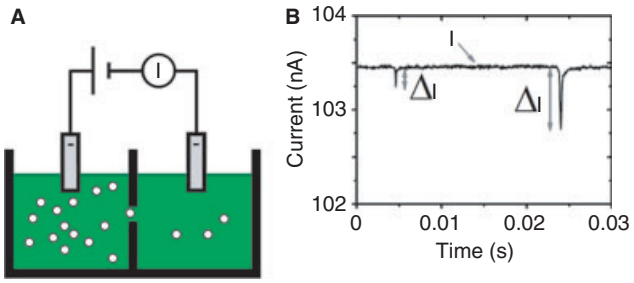

Fig. 4. Resistive pulse sensing. (A) Schematic representation of resistive pulse sensing (RPS). The instrument consists of two fluid cells divided by an insulating membrane containing a single pore. In each fluid cell, an electrode is immersed to drive an ionic current through the pore. (B) Current *I* vs. time for vesicles from plasma diluted 1:10 with PBS as measured by RPS (Izon qNano, Christchurch, New Zealand). The two downward spikes *ΔI* are due to single vesicles successively passing through the pore.

verified using liposomes of known diameter (personal communication, Izon Science Ltd). The sample volume can be as low as 10 μL. By applying a pressure difference between the fluid cells, pressure-driven flow dominates the flow caused by electro-osmosis, electrophoresis, and diffusion. The count rate is related to the concentration of vesicles using beads of known concentration [50].

Applicability and limitations Because the relative change in current is proportional to the volume of the particle, RPS can accurately determine the diameter of single particles. For example, we have sized 102 nm and 203 nm NIST traceable polystyrene beads with an accuracy of 2% (data not shown). The size range that can be detected is bound by the pore size at the upper limit and by the smallest detectable resistance change at the lower limit, which is approximately 20% of the pore diameter. For example, a pore with a diameter of 400 nm is capable of sizing vesicles ranging from ~80 to < 400 nm in diameter. Flexible pores with adjustable pore sizes can be used to increase the detection range.

A practical limitation of measuring biological samples with RPS is pore clogging. The pore may get clogged due to the accumulation of high molecular weight proteins such as fibrinogen or von Willebrand Factor, or due to particles larger than the pore, for example, apoptotic blebs, small cells, and aggregates of vesicles or calibration beads. It should be mentioned that the calibration beads may form aggregates soon after dilution in PBS. If pore clogging occurs, the measurement has to be paused for pore unclogging. Both unclogging and contaminants such as proteins sticking to the pore may alter the dimensions of the sensing zone. Consequently, the calibration measurement should be verified. Sample preparation to remove vesicles larger than the pore and to reduce the concentration of proteins is therefore critical.

From our experience, mainly due to pore clogging, the measurement time ranges from 30 min to 1 h per biological sample, making the qNano a research tool rather than a tool suitable for clinical routine analysis.

New developments To automatically clean a clogged pore, a resistive pulse sensor with integrated ultrasound transducer is in development (personal communication, Izon Science Ltd). While this is a promising development for cleaning pores, careful testing is needed because sonication may cause breakdown of vesicles.

Recently, the dependency of the resistance of the pore on the particle position, particle size, and the dimensions of the pore was analytically described [51], allowing determination of the zeta potential of single particles.

Nanoparticle tracking analysis

Nanoparticle tracking analysis (NTA), commercialized by Nanosight Ltd (Amesbury, UK), measures the absolute size distribution of vesicles ranging from ~50 nm to 1 μm in diameter. Vesicles in suspension are illuminated by a laser beam and scatter light or exhibit fluorescence. A dark-field microscope is used to determine the position of single vesicles, which are continuously moving due to Brownian motion. For each vesicle, the movements are tracked and the mean squared velocity is calculated. Because the mean squared velocity of the Brownian motion depends on the particle diameter, an absolute size distribution of vesicles in suspension can be obtained after the system has been calibrated with beads of known concentration [12]. NTA can determine the zeta potential by applying an electric field across the suspension and measuring the velocity of single vesicles due to electrophoresis [52]. With fluorescent labeling, NTA can be used to determine the size of a subgroup of vesicles [53].

Applicability and limitations With a typical measurement time of several minutes, NTA is convenient to use. The visualization of samples provides real-time feedback on the aggregation of particles and on the possible presence of cells after vesicle isolation. Furthermore, NTA is capable of detecting single vesicles with a diameter as low as 50 nm based on light scattering and detecting even smaller vesicles if labeled with at least a single quantum dot [12].

Uncertainty in the position determination and the linear relationship between the reciprocal diameter of a particle and its diffusion coefficient lead to broadening of the obtained size distribution. Consequently, two populations can only be resolved if their particle diameters differ by at least 1.5-fold. In addition, the accuracy of the determination of the concentration of vesicles or a mixture of beads with different diameters is strongly affected by their size and refractive index, the uniformity and power of illumination, and the camera settings. For example, in a heterogeneous mixture of polystyrene beads (Thermo Fisher Scientific, Waltham, MA, USA), the concentration of 596 nm beads is overestimated more than 7-fold by NTA (data not shown). For vesicles, this problem can be contained by calibrating the instrument with 100 nm silica beads of known concentration [54], selecting a vesicle concentration between 10^8 and 10^9 vesicles mL^{-1}, and optimizing the camera gain [55]. When studying vesicles in biological samples, it is recommended to perform two measurements. First, the sample is undiluted and a low camera gain is used to track the relatively low concentration of large vesicles. Second, the sample is diluted and the most sensitive camera setting is used to track the relatively high concentration of small vesicles.

NTA generates 1–2 GB of video data per measurement, which means that data backup and handling require considerable time and storage capacity. The generated video data require sophisticated data processing, involving multiple operations and variables. Although there is a tendency toward the automatic determination of these variables, substantial operator skill is required.

New developments An instrument that supports dual labeling by utilizing two fluorescence channels is under development, as well as high throughput solutions, such as an autosampler and an extension capable of automatically diluting samples (personal communication Nanosight Ltd).

Beyond state of the art: detection of vesicles by specialized techniques

Raman microspectroscopy

Raman spectroscopy is based on the detection of inelastic light scattering and is used to study the structure and chemical composition of macromolecules inside single living cells [56]. The sample is illuminated by monochromatic laser light. When the light is inelastically scattered by the sample, the wavelength shifts due to an energy gain or loss associated with molecular vibrations in the sample. Because this wavelength shift is molecule specific, Raman spectroscopy allows label-free examination. With Raman microspectroscopy, the probe volume is typically $< 1\ \mu m^3$, which overlaps with the dimension of vesicles. Fig. 5 shows the Raman spectrum of a single vesicle isolated from an erythrocyte concentrate by differential centrifugation. This spectrum was obtained using a confocal Raman microspectrometer, in which a 647-nm laser with a power of 100 mW was focused on a probe volume of $0.3\ \mu m^3$ [57]. Due to the high irradiance, the vesicle was optically trapped in the laser beam. The peaks in the spectrum are specific to the chemical bonds and symmetry of the molecules. Because the amplitude of the signal is linearly proportional to the number of molecules, Raman microspectroscopy is a quantitative technique. Recently,

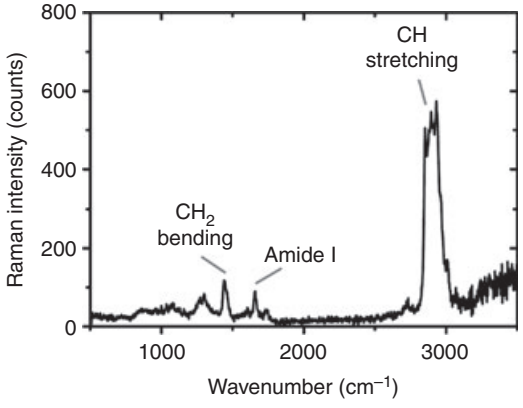

Fig. 5. Raman spectrum of a single erythrocyte-derived vesicle The Raman spectrum of a single erythrocyte vesicle is shown in suspension after subtraction of the background spectrum of the medium. The peaks reveal specific chemical bonds, which are present in this vesicle. For instance, the peak at 1654 cm^{-1} is characteristic for Amide I, the peak at 1440 cm^{-1} is characteristic for methylene (CH_2) bending, and the peak at 2947 cm^{-1} is characteristic for hydrocarbon (C–H) stretching.

Raman microspectroscopy was applied to study vesicles of *Dictyostelium discoideum*, a convenient model to study eukaryotic vesicles [58]. Without labeling, at least two different types of vesicles were identified, illustrating that Raman microspectroscopy allows label-free distinction between single vesicles of different composition.

Applicability and limitations Raman microspectroscopy is a relatively expensive and specialized method with limited availability. In addition, a measurement takes considerable time, because trapping is a stochastic process and because the intensity of Raman scattering is weak compared with Rayleigh scattering. Consequently, acquisition times in the order of seconds per vesicle are required. Thus, with the current state of the art, obtaining Raman spectra from 1000 vesicles would take hours.

New developments To obtain simultaneous information on the size, concentration, and chemical composition of single vesicles in suspension without fluorescence antibody labeling, we will combine Raman microspectroscopy with RPS (qNano). The sample stream in the qNano will force vesicles through the focused laser beam to reduce measurement time.

Micro NMR

Nuclear magnetic resonance (NMR) can be used to measure the magnetic susceptibility of a sample, that is, the degree of sample magnetization in response to an applied magnetic field. In general, biological samples have negligible magnetic susceptibility [59], but using magnetic nanoparticles conjugated to an antibody, the presence of an antigen exposed on a vesicle can be detected. The miniaturized micro nuclear magnetic resonance (μNMR) system [60] is a lab-on-a-chip NMR device capable of measuring the large contrast in magnetic susceptibility between biological samples and magnetic nanoparticles. Vesicles with a diameter of 50–150 nm are loaded into multiple parallel chambers, each chamber containing a 50 nm pore size filter to prevent the vesicles from leaving the chamber while allowing reagents to pass through the chamber. Each chamber is labeled with a different antibody conjugated to 38 nm ferrite nanoparticles [61]. The number of vesicles present in a chamber is estimated by labeling vesicles in one of the chambers with an antibody directed against CD63, a tetraspanin exposed on many vesicles. The magnetic susceptibility detected in the parallel sample chambers is normalized for the CD63 signal to account for variations in the number of vesicles in each chamber. The μNMR system detects the presence of magnetic nanoparticles in the sample chamber with great sensitivity. For example, the CD63 signal from 10^4 vesicles could be detected, which is claimed to be a 1000-fold more sensitive than ELISA. The sample size is 1 μL per chamber and the measurement time approximately 1 h.

Applicability and limitations The μNMR has been applied to detect glioblastome multiforme (GBM) vesicles in plasma of mice and humans [60]. μNMR provides no information on *single* vesicles. Nevertheless, the high sensitivity of this method beholds great promise to detect rare vesicles, such as tumor-derived vesicles in plasma samples. For example, in GBM, vesicles may be a new serological biomarker in a field where the currently available biomarkers are insensitive and expensive to measure [60]. The number of different antigens that can be detected can be expanded by loading and labeling more sample chambers. Changing the filter pore sizes used for sample preparation may allow biochemical characterization of vesicles of different sizes.

Small-angle X-ray scattering (SAXS)

The small-angle X-ray scattering method is based on the elastic scattering of X-ray photons at low angles. In contrast to protein crystallography, where the atomic structure of macromolecules is determined by collecting the scattering pattern at wide angles, SAXS can provide structural information on nanomaterials, for example, the bilayer thickness of vesicles, in the 1 nm to 100 nm size range. For sufficiently monodisperse nanoparticles, a traceable size determination is possible [62,63]. SAXS measurements require monochromatic X-ray with a wavelength below 1 nm, which is perfectly suited to probe nanomaterials. The forward scattered radiation from the sample is recorded at small angles (typically up to about 3°) with a large area pixel detector placed at variable distance (typically 1 m to 4 m) from the sample. The one-dimensional scattering curves as function of the scattering angle are obtained by radial averaging of the two-dimensional scattering pattern. The momentum transfer depends on the scattering angle and wavelength, and provides information for dimensional characterization.

SAXS was already applied to describe the organization of the lipid bilayer of various vesicles of synthetic and natural origin [64–67], for example, Castorph *et al.* studied the structure of synaptic vesicles using SAXS and obtained detailed information on size, density, and composition [67]. Because extracellular vesicles are enclosed by a phospholipid bilayer membrane, SAXS can provide detailed information on their phospholipid bilayer structure and embedded transmembrane proteins, which are both in the nm range. In the case of objects such as vesicles with overall diameter below 100 nm, the scattering of the whole vesicle appears at low momentum transfer, enabling the characterization of the vesicle size and shape. These features can be demonstrated for synthetic phospholipid vesicles, which are commonly used as model systems for biological membranes and as drug delivery vehicles. The scattered intensity of a liposome system with a diameter of 100 nm is shown in Fig. 6.

Applicability and limitations While SAXS has been applied in soft matter science, two main limitations have to be considered. The scattered intensity relates to the sixth power of the radius in the case of spherical particles, causing large differences in the scattering signal from particles with different sizes. As a consequence, the scattering from samples containing vesicles with large differences in diameter may lead to ambiguous determination of the size distribution. As small-angle scattering results from electron density discontinuities, the second limitation is the decrease in the scattered intensity with decreasing (electron) density contrast. Therefore, SAXS characterization of biological materials that have a low electron density contrast relative to the aqueous media requires very intense monochromatic X-rays, which are usually available only at synchrotron radiation facilities. Fig. 7A shows the electron storage ring BESSY II with 250 meter circumference in Berlin, together with the laboratory of PTB [68]. Beamline 2a in this figure is the 40 meter long four-crystal monochromator beamline. The SAXS set-up of Helmholtz-Zentrum Berlin is installed at this beamline as shown in Fig. 7B. The monochromatized and collimated X-ray beam interacts with the sample placed in a vacuum chamber.

Anomalous Small-angle X-ray scattering (ASAXS)

Biological samples exhibit complex small-angle scattering curves due to their multicomponent nature and hierarchical structural characteristics. Identifying each scattering contribution is the main challenge in the interpretation of SAXS curve of samples such as vesicles. Separation of the scattering contributions of the different constituents of this complex system can be achieved using anomalous small-angle X-ray scattering (ASAXS). Because every chemical element has characteristic X-ray absorption edges, the presence of each element can be detected by recording scattering curves at appropriate wavelengths. In case of vesicles,

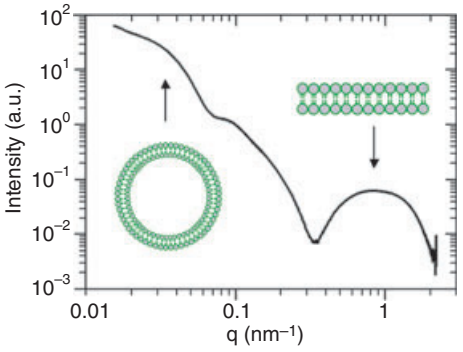

Fig. 6. Scattered intensity of phospholipid vesicles by SAXS The scattering intensity curve of 100 nm phospholipid vesicles provides information about the size (low q) and bilayer thickness (high q) of the vesicles. The relevant physical quantity for the dimensional characterization is the momentum transfer q, which is related to and wavelength λ and scattering angle θ by $q = 4\pi/\lambda \sin \theta$.

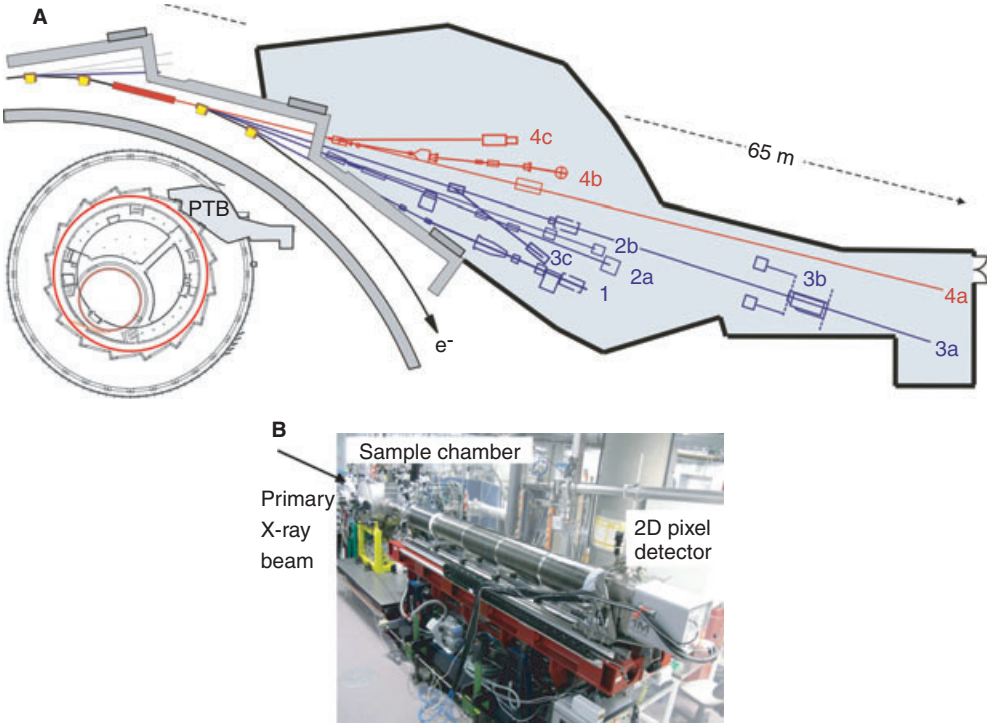

Fig. 7. Measuring vesicles by Small-Angle X-ray Scattering A. The layout of the PTB laboratory at the BESSY II synchrotron radiation facility in Berlin (Germany). The ring circumference is 250 m. B. The generated X-ray photons pass the four-crystal monochromator beamline.

ASAXS can identify the contribution from proteins (sulfur), phospholipids, and nucleic acids (phosphorus). For example, the distribution of proteins between the inner and outer side of the phospholipid bilayer can be determined, as well as the thickness of the bilayer. Because the absorption edges of relevant elements of vesicles are at photon energies below 3 keV where the penetration length of X-ray is limited, the commonly used glass capillaries have to be replaced by a dedicated sample cell with thin (< 1 μm) silicon nitride windows. The sample cell and the detector have to be placed in vacuum. A vacuum-compatible large area X-ray detector has become only recently available and will be used to study vesicles present in human body fluids in the Metves project (www.metves.eu) [69].

Discussion

Vesicles have become firmly established entities, a fact illustrated by founding of the International Society of Extracelluar Vesicles (www.isev.org). Only recently it has become apparent, however, by application of novel commercially available technologies such as NTA and RPS, that many vesicles are extremely small with a diameter of less than 100 nm. The straightforward detection of such vesicles is hampered by their small size, high concentration, low refractive index, and heterogeneity in size, composition, and morphology.

In this review, we have shown that application of commercially available methods for vesicle detection requires background knowledge of the underlying principles of such methods, so that obtained results can be appropriately interpreted. Also, measurement results on vesicles by application of such methods have been insufficiently compared with each other, and at present, standard populations of vesicles are being studied using transmission electron microscopy, flow cytometry (BD FACSCalibur, Apogee A50-micro), NTA (Nanosight NS500, Nanosight LM-10), and RPS (Izon qNano, personal communication). We hope to learn from such studies what the capabilities and limitations are of the methods [2] and what the true concentration and diameter are of vesicles in biological fluids.

We have also shown that exciting attempts are now being made to explore the cutting edge of physical and biochemical know-how to improve the detection of vesicles. Some of the methods, such as SAXS, can provide the absolute size or size distribution of vesicles in suspension, whereas other methods, such as Raman microspectroscopy, have the potential to obtain biochemical information, such as cellular origin, on the level of single vesicles directly in suspension without labeling.

For the vesicle field to leap forward, the detection limits of existing technologies need to be pushed further or the detection limits need to be improved by combining technologies and developing new technologies. With more sensitive technology, we expect to gain a growing insight into the composition, biological and clinical relevance of vesicles in health and disease.

Acknowledgements

Part of this manuscript is funded by European Metrology Research Programme (EMRP), which is jointly funded by the EMRP participating countries within EURAMET and the European Union. We thank Prof. Dr. A. Sturk and Prof. Dr. T. G. van Leeuwen for their excellent assistance with constructing and writing this manuscript.

Disclosure of Conflicts of Interest

The authors state that they have no conflict of interest.

References

1 van der Pol E, Boing AN, Harrison P, Sturk A, Nieuwland R. Classification, functions, and clinical relevance of extracellular vesicles. *Pharmacol Rev* 2012; **64**: 676–705.
2 van der Pol E, Hoekstra AG, Sturk A, Otto C, van Leeuwen TG, Nieuwland R. Optical and non-optical methods for detection and characterization of microparticles and exosomes. *J Thromb Haemost* 2010; **8**: 2596–607.
3 Yuana Y, Bertina RM, Osanto S. Pre-analytical and analytical issues in the analysis of blood microparticles. *Thromb Haemost* 2011; **105**: 396–408.
4 Lacroix R, Judicone C, Poncelet P, Robert S, Arnaud L, Sampol J, Dignat-George F. Impact of pre-analytical parameters on the measurement of circulating microparticles: towards standardization of protocol. *J Thromb Haemost* 2012; **10**: 437–46.
5 van der Zee PM, Biro E, Ko Y, De Winter RJ, Hack CE, Sturk A, Nieuwland R. P-selectin- and CD63-exposing platelet microparticles reflect platelet activation in peripheral arterial disease and myocardial infarction. *Clin Chem* 2006; **52**: 657–64.
6 van der Pol E, van Leeuwen TG, Nieuwland R. An overview of novel and conventional methods to detect extracellular vesicles. In: Sargent I, Harrison P, eds. *Micro/Nanovesicles and Exosomes in Health and Disease*, 1st edn. Singapore: Pan Stanford, 2013.
7 Connor DE, Exner T, Ma DD, Joseph JE. The majority of circulating platelet-derived microparticles fail to bind annexin V, lack phospholipid-dependent procoagulant activity and demonstrate greater expression of glycoprotein Ib. *Thromb Haemost* 2010; **103**: 1044–52.
8 Gyorgy B, Modos K, Pallinger E, Paloczi K, Pasztoi M, Misjak P, Deli MA, Sipos A, Szalai A, Voszka I, Polgar A, Toth K, Csete M, Nagy G, Gay S, Falus A, Kittel A, Buzas EI. Detection and isolation of cell-derived microparticles are compromised by protein complexes resulting from shared biophysical parameters. *Blood* 2011; **117**: e39–48.
9 Hexley P, Robinson CT, Osterburg AR, Babcock GF. Circulating microparticles do not all share biophysical light scatter properties with immune complexes when analyzed by flow cytometry. *Blood* 2012; **120**: 1528–9.
10 Amabile N, Renard JM, Caussin C, Boulanger CM. Circulating immune complexes do not affect microparticle flow cytometry analysis in acute coronary syndrome. *Blood* 2012; **119**: 2174–5.
11 Larson MC, Luthi MR, Hogg N, Hillery CA. Calcium-phosphate microprecipitates mimic microparticles when examined with flow cytometry. *Cytometry A* 2012; **83**: 242–50.
12 Dragovic RA, Gardiner C, Brooks AS, Tannetta DS, Ferguson DJ, Hole P, Carr B, Redman CW, Harris AL, Dobson PJ, Harrison P, Sargent IL. Sizing and phenotyping of cellular vesicles using Nanoparticle Tracking Analysis. *Nanomedicine* 2011; **7**: 780–8.
13 Aass HC, Ovstebo R, Troseid AM, Kierulf P, Berg JP, Henriksson CE. Fluorescent particles in the antibody solution result in false TF- and CD14-positive microparticles in flow cytometric analysis. *Cytometry A* 2011; **79**: 990–9.
14 Berckmans RJ, Nieuwland R, Tak PP, Boing AN, Romijn FP, Kraan MC, Breedveld FC, Hack CE, Sturk A. Cell-derived microparticles in synovial fluid from inflamed arthritic joints support coagulation exclusively via a factor VII-dependent mechanism. *Arthritis Rheum* 2002; **46**: 2857–66.
15 Boilard E, Nigrovic PA, Larabee K, Watts GF, Coblyn JS, Weinblatt ME, Massarotti EM, Remold-O'Donnell E, Farndale RW, Ware J, Lee DM. Platelets amplify inflammation in arthritis via collagen-dependent microparticle production. *Science* 2010; **327**: 580–3.
16 Yuana Y, Oosterkamp TH, Bahatyrova S, Ashcroft B, Garcia RP, Bertina RM, Osanto S. Atomic force microscopy: a novel approach to the detection of nanosized blood microparticles. *J Thromb Haemost* 2010; **8**: 315–23.
17 Ashcroft BA, de Sonneville, Yuana Y, Osanto S, Bertina R, Kuil ME, Oosterkamp TH. Determination of the size distribution of blood microparticles directly in plasma using atomic force microscopy and microfluidics. *Biomed Microdevices* 2012; **14**: 641–9.
18 Lacroix R, Robert S, Poncelet P, Kasthuri RS, Key NS, Dignat-George F. Standardization of platelet-derived microparticle enumeration by flow cytometry with calibrated beads: results of the International Society on Thrombosis and Haemostasis SSC Collaborative workshop. *J Thromb Haemost* 2010; **8**: 2571–4.
19 van der Pol E, van Gemert MJ, Sturk A, Nieuwland R, van Leeuwen TG. Single versus swarm detection of microparticles and exosomes by flow cytometry. *J Thromb Haemost* 2012; **10**: 919–30.
20 Harrison P, Gardiner C. Invisible vesicles swarm within the iceberg. *J Thromb Haemost* 2012; **10**: 916–18.
21 Bohren CF, Huffman DR. *Absorption and Scattering of Light by Small Particles*. New York: Wiley, 1983.
22 Konokhova AI, Yurkin MA, Moskalensky AE, Chernyshev AV, Tsvetovskaya GA, Chikova ED, Maltsev VP. Light-scattering flow cytometry for identification and characterization of blood microparticles. *J Biomed Opt* 2012; **17**: 057006.
23 Perez-Pujol S, Marker PH, Key NS. Platelet microparticles are heterogeneous and highly dependent on the activation mechanism: studies using a new digital flow cytometer. *Cytometry A* 2007; **71**: 38–45.
24 Robert S, Poncelet P, Lacroix R, Arnaud L, Giraudo L, Hauchard A, Sampol J, Dignat-George F. Standardization of platelet-derived microparticle counting using calibrated beads and a Cytomics FC500 routine flow cytometer: a first step towards multicenter studies? *J Thromb Haemost* 2009; **7**: 190–7.
25 Steen HB. Flow cytometer for measurement of the light scattering of viral and other submicroscopic particles. *Cytometry A* 2004; **57**: 94–9.
26 Robert S, Poncelet P, Lacroix R, Raoult D, Dignat-George F. More on: calibration for the measurement of microparticles: value of calibrated polystyrene beads for flow cytometry-based sizing of biological microparticles. *J Thromb Haemost* 2011; **9**: 1676–8.
27 Vorauer-Uhl K, Wagner A, Borth N, Katinger H. Determination of liposome size distribution by flow cytometry. *Cytometry* 2000; **39**: 166–71.
28 Lacroix R, Robert S, Poncelet P, Dignat-George F. Overcoming limitations of microparticle measurement by flow cytometry. *Semin Thromb Hemost* 2010; **36**: 807–18.
29 Chandler WL, Yeung W, Tait JF. A new microparticle size calibration standard for use in measuring smaller microparticles using a new flow cytometer. *J Thromb Haemost* 2011; **9**: 1216–24.
30 Mullier F, Bailly N, Chatelain C, Dogne JM, Chatelain B. More on: calibration for the measurement of microparticles: needs, interests, and limitations of calibrated polystyrene beads for flow

cytometry-based quantification of biological microparticles. *J Thromb Haemost* 2011; **9**: 1679–81.
31 van Manen HJ, Verkuijlen P, Wittendorp P, Subramaniam V, van den Berg TK, Roos D, Otto C. Refractive index sensing of green fluorescent proteins in living cells using fluorescence lifetime imaging microscopy. *Biophys J* 2008; **94**: L67–9.
32 Zwicker JI. Impedance-based flow cytometry for the measurement of microparticles. *Semin Thromb Hemost* 2010; **36**: 819–23.
33 Zhang H, Chon CH, Pan X, Li D. Methods for counting particles in microfluidic applications. *Microfluid Nanofluid* 2009; **7**: 739–49.
34 Wu X, Kang Y, Wang YN, Xu D, Li D. Microfluidic differential resistive pulse sensors. *Electrophoresis* 2008; **29**: 2754–9.
35 Wu X, Chon CH, Wang YN, Kang Y, Li D. Simultaneous particle counting and detecting on a chip. *Lab Chip* 2008; **8**: 1943–9.
36 Nieuwenhuis J, Kohl F, Bastemeijer J, Sarro P, Vellekoop M. Integrated coulter counter based on 2-dimensional liquid aperture control. *Sens Actuators B Chem* 2004; **102**: 44–50.
37 Rodriguez-Trujillo R, Mills C, Samitier J, Gomila G. Low cost micro-coulter counter with hydrodynamic focusing. *Microfluid Nanofluid* 2007; **3**: 171–6.
38 Nolan JP, Stoner SA. A trigger channel threshold artifact in nanoparticle analysis. *Cytometry A* 2013; **83**: 301–5.
39 van der Vlist EJ, Nolte-'t Hoen EN, Stoorvogel W, Arkesteijn GJ, Wauben MH. Fluorescent labelling of nano-sized vesicles released by cells and subsequent quantitative and qualitative analysis by high-resolution flow cytometry. *Nat Protoc* 2012; **7**: 1311–26.
40 Hoen EN, van der Vlist EJ, Aalberts M, Mertens HC, Bosch BJ, Bartelink W, Mastrobattista E, van Gaal EV, Stoorvogel W, Arkesteijn GJ, Wauben MH. Quantitative and qualitative flow cytometric analysis of nanosized cell-derived membrane vesicles. *Nanomedicine* 2012; **8**: 712–20.
41 Clark NA, Lunack JH, Benedek GB. A study of Brownian motion using light scattering. *Am J Phys* 1970; **38**: 575–85.
42 Dieckmann Y, Colfen H, Petri-Fink A. Particle size distribution measurements of maganese-doped ZnS nanoparticles. *Anal Chem* 2009; **81**: 3889–95.
43 Bryant G, Abeynayake C, Thomas JC. Improved particle size distribution measurements using multiangle dynamic light scattering. 2. Refinements and applications. *Langmuir* 1996; **12**: 6224–8.
44 Filella M, Zhang JW, Newman ME, Buffle J. Analytical applications of photon correlation spectroscopy for size distribution measurements of natural colloidal suspensions. *Colloids Surf A Physicochem Eng Asp* 1997; **120**: 27–46.
45 Hoo CM, Starostin N, West P, Mecartney ML. A comparison of atomic force microscopy (AFM) and synamic light scattering (DLS) methods to characterize nanoparticle size distributions. *J Nanopart Res* 2008; **10**: 89–96.
46 Lawrie AS, Albanyan A, Cardigan RA, Mackie IJ, Harrison P. Microparticle sizing by dynamic light scattering. *Vox Sang* 2009; **96**: 206–12.
47 Xu Y, Nakane N, Maurer-Spurej E. Novel test for microparticles in platelet-rich plasma and platelet concentrates using dynamic light scattering. *Transfusion* 2011; **51**: 363–70.
48 Vogel R, Wilmott G, Kozak DM, Roberts GS, Anderson W, Groenewegen L, Glossop B, Barnett A, Turner A, Trau M. Quantitative sizing of nano/microparticles with tunable elastomeric pore sensor. *Anal Chem* 2011; **83**: 3499–506.
49 Ito T, Sun L, Henriquez RR, Crooks RM. A carbon nanotube-based coulter nanoparticle counter. *Acc Chem Res* 2004; **37**: 937–45.
50 Roberts GS, Yu S, Zeng Q, Chan LC, Anderson W, Colby AH, Grinstaff MW, Reid S, Vogel R. Tunable pores for measuring concentrations of synthetic and biological nanoparticle dispersions. *Biosens Bioelectron* 2012; **31**: 17–25.
51 Kozak D, Anderson W, Vogel R, Chen S, Antaw F, Trau M. Simultaneous size and zeta-potential measurements of individual nanoparticles in dispersion using size-tunable pore sensors. *ACS Nano* 2012; **6**: 6990–7.
52 Carr B, Hole P, Malloy A, Weld A, Nelson P, Smith J, *et al*. The real-time, simultaneous measurement of size, surface charge and fluorescence of populations of nanoparticles in liquids. Proceedings of: Particulate Systems Analysis, Stratford-upon-Avon, UK, September 2–4, 2008.
53 Braeckmans K, Buyens K, Bouquet W, Vervaet C, Joye P, De VF, Plawinski L, Doeuvre L, Angles-Cano E, Sanders NN, Demeester J, De Smedt SC. Sizing nanomatter in biological fluids by fluorescence single particle tracking. *Nano Lett* 2010; **10**: 4435–42.
54 Gardiner C, Ferreira YJ, Dragovic RA, Redman CWG, Sargent IL. Extracellular vesicle sizing and enumeration by nanoparticle tracking analysis. *J Extr Vesi* 2013; **2**: 19671.
55 Malloy A, Carr B. The Halo (TM) system. *Part Part Syst Charact* 2006; **2006**: 197–204.
56 Puppels GJ, de Mul FF, Otto C, Greve J, Robert-Nicoud M, Arndt-Jovin DJ, Jovin TM. Studying single living cells and chromosomes by confocal Raman microspectroscopy. *Nature* 1990; **347**: 301–3.
57 Pully VV, Lenferink ATM, Otto C. Time-lapse Raman imaging of single live lymphocytes. *J Raman Spectrosc* 2011; **42**: 167–73.
58 Tatischeff I, Larquet E, Falcón-Pérez JM, Turpin P-Y, Kurglik SG. Fast characterisation of cell-derived extracellular vesicles by nanoparticles tracking analysis, cryo-electron microscopy, and Raman tweezers microspectroscopy. *J Extr Vesi* 2012; **1**: 1–11.
59 Shao H, Yoon TJ, Liong M, Weissleder R, Lee H. Magnetic nanoparticles for biomedical NMR-based diagnostics. *Beilstein J Nanotechnol* 2010; **1**: 142–54.
60 Issadore D, Min C, Liong M, Chung J, Weissleder R, Lee H. Miniature magnetic resonance system for point-of-care diagnostics. *Lab Chip* 2011; **11**: 2282–7.
61 Shao H, Chung J, Balaj L, Charest A, Bigner DD, Carter BS, Hochberg FH, Breakefield XO, Weissleder R, Lee H. Protein typing of circulating microvesicles allows real-time monitoring of glioblastoma therapy. *Nat Med* 2012; **18**: 1835–40.
62 Gleber G, Cibik L, Haas S. Traceble size determination of PMMA nanoparticles based on Small Angle X-ray Scattering (SAXS). *J Phys Conf Ser* 2010; **247**(2010): 012027.
63 Krumrey M, Gleber G, Scholze F, Wernecke J. Synchrotron radiation-based x-ray reflection and scattering techniques for dimensional nanometrology. *Meas Sci Technol* 2011; **22**: 094032.
64 Bouwstra JA, Gooris GS, Bras W, Talsma H. Small angle X-ray scattering: possibilities and limitations in characterization of vesicles. *Chem Phys Lipids* 1993; **64**: 83–98.
65 Brzustowicz MR, Brunger AT. X-ray scattering from unilamellar lipid vesicles. *J Appl Crystallogr* 2005; **38**: 126–31.
66 Hirai M, Iwase H, Hayakawa T, Koizumi M, Takahashi H. Determination of asymmetric structure of ganglioside-DPPC mixed vesicle using SANS, SAXS, and DLS. *Biophys J* 2003; **85**: 1600–10.
67 Castorph S, Riedel D, Arleth L, Sztucki M, Jahn R, Holt M, Salditt T. Structure parameters of synaptic vesicles quantified by small-angle x-ray scattering. *Biophys J* 2010; **98**: 1200–8.
68 Beckhoff B, Gottwald A, Klein R, Krumrey M, Müller R, Richter M, Scholze F, Thornagel R, Ulm G. A quarter century of metrology using synchotron radiation by PTB in Berlin. *Physica Status Solidi* 2009; **B246**: 1415–34.
69 Donath T, Brandstetter S, Cibik L, Commichau S, Hofer P, Krumrey M, Lüthi B, Marggraf S, Müller P, Schneebeli M, Schulze-Briese C, Wernecke J. Characterization of the PILATUS photon-counting pixel detector for X-ray energies from 1.75 keV to 60 keV. *J of Physics*: conference series 2013; in print.